EBK quantization of quasi-energies

1992 J. Phys. A: Math. Gen. 25 6761

(http://iopscience.iop.org/0305-4470/25/24/027)

J. Phys. A: Math. Gen. 25 (1992) 6761–6777. Printed in the UK

EBK quantization of quasi-energies

F Bensch†, H J Korsch†, B Mirbach† and N Ben-Tal‡

† Fachbereich Physik, Universität Kaiserslautern D-6750 Kaiserslautern, Federal Republic of Germany

‡ Department of Chemistry, Technion Israel Institute of Technology, Haifa, 32000, Israel

Received 10 April 1992

Abstract. The semiclassical Einstein–Brillouin–Keller vortex tube quantization for the quasi-energies in time-periodic Hamiltonians is studied for typical systems, when the vortex tubes of the quantizing tubes may have complicated structures in extended phase space. Numerical application to a periodically driven Duffing (quartic) oscillator yields semiclassical quasi-energies in excellent agreement with the exact quantum mechanical ones for the regular states.

1. Introduction

The intricate interrelation between *nonlinear (chaotic) classical dynamics* and *linear* quantum dynamics appears to be of current interest. In particular the semiclassical quantization of conservative systems of n degrees of freedom has been studied in much detail. The semiclassical Einstein–Brillouin–Keller (EBK) quantization (see the review articles [1, 2]) is based on the existence of invariant tori in classical phase space and was originally only defined for integrable systems. For weakly disturbed integrable systems adiabatic switching methods (see e.g. [3]) as well as interpolation techniques have been developed (see [4, 5] and [6] with references therein). They allow an EBK quantization for non-integrable systems in phase space regimes where invariant tori still exist. In strongly chaotic regimes, however, tori are rare or fail to exist at all. For such cases semiclassical periodic orbit theories as developed, for example, by Gutzwiller [7] are currently under investigation.

A theoretically attractive reduction in the number of degrees of freedom can be achieved by considering one-dimensional time-periodic systems, which are considerably simpler to study than, for example, two-dimensional conservative ones. They retain, however, most of the characteristic chaotic dynamics. In addition, such systems model the dynamics of atoms or molecules in strong laser fields, which opens interesting experimental perspectives. The dynamics may depend sensitively on system parameters, like field strength or laser frequency, which can be varied to explore the manifestion of *classical chaotic phenomena in quantum mechanics experimentally.*

The present paper contributes to the understanding of the structure of the quasi-energy spectrum of such time-periodic systems by investigating the semiclassical EBK quantization of the regular part of the spectrum. Let us recall that the quasi-energy states for the Hamiltonian

$$\hat{H}(p, q, t) = \hat{H}(p, q, t + T) \tag{1}$$

0305-4470/92/246761+17$07.50

are defined by

$$\psi_\alpha(q,t) = \mathrm{e}^{-\mathrm{i}\varepsilon_\alpha t/\hbar}\, u_\alpha(q,t) \tag{2}$$

with T-periodic functions $u_\alpha(q,t)$. The quasi-energies, ε_α, are defined up to an integer multiple of $\hbar\omega = \hbar 2\pi/T$. In section 2 we give a short resumé of the semiclassical EBK theory for quasi-energies, which relies heavily on the recent work by Breuer and Holthaus [8].

The procedure for numerical quantization is addressed in section 2.1 and results are presented in section 4 for a harmonically driven quartic oscillator. This system, which is also known as a frictionless Duffing or Ueda oscillator [9, 10] has been studied recently in quantum mechanics [11, 12] (see also [13] for a quantum study of the kicked quartic oscillator). It was found in [11, 12] that the quantum quasi-energy states quite naturally fall into two classes, namely extended and localized states, which closely parallels the classical behaviour. The quasi-energy states, which are found to be exponentially localized in the space of states of the field-free Hamiltonian, are localized in the regular region of classical phase space, whereas the extended states mostly populate the chaotic phase space region, as demonstrated by the quantum Husimi phase space densities. In the present article it is shown that this correspondence can be sharpened: all the states classified as localized in the previous quantum computation could be obtained by EBK vortex tube quantization, i.e. they are supported by regular classical dynamics.

2. Semiclassical quantum conditions

The semiclassical approximation for time-periodic systems can be achieved by constructing an extended phase space in which the system appears as time-independent so that the well known EBK quantization can be implemented. A comprehensive description of this theory can be found in [8]. Here we will confine ourselves to the one-dimensional time-periodic case and put emphasis on the difference to time-independent two-dimensional systems. Suppose we have a classical Hamiltonian

$$H(p,q,t) = H(p,q,t+T) \tag{3}$$

with period $T = 2\pi/\omega$. Such a Hamiltonian is not usually an integral of motion. However, by regarding t as a variable and introducing an additional canonical momentum p_t, a new conserved Hamiltonian $\widetilde{H}$, the quasi-energy function, can be constructed in an extended phase space $\{q,p,t,p_t\}$ by

$$\widetilde{H}(q,p,t,p_t) = H(q,p,t) + p_t. \tag{4}$$

The new p_t is the conjugated momentum to the time coordinate, as can be seen immediately by utilizing the conservation of $\widetilde{H}$ (we have now to distinguish between the time variable t and the time parametrizing the Hamiltonian flow in the extended phase space; the latter will be denoted by s in the following).

$$0 = \frac{\mathrm{d}\widetilde{H}}{\mathrm{d}s} \longrightarrow \dot{p}_t = -\frac{\mathrm{d}H}{\mathrm{d}s} = -\frac{\partial H}{\partial s}. \tag{5}$$

The symplectic two-form in extended phase space is hence given by

$$\omega^2 = p \wedge \mathrm{d}q + p_t \wedge \mathrm{d}t. \tag{6}$$

It is important to note that invariant surfaces in such systems are not topologically two-dimensional tori but non-compact cylinders. In the case of a time-periodic system, however, we can regard t as an angle variable by identifying t and $t + T$. In the case of an integrable system the phase space is completely filled with such invariant tori. The EBK quantization condition selects a countable number of tori by requiring

$$I_i = \frac{1}{2\pi} \oint_{\gamma_i} p\,\mathrm{d}q + p_t\,\mathrm{d}t = \hbar(n_i + \tfrac{1}{4}\mu_i) \qquad n_i \in \mathbb{Z},\ i = 1,2 \tag{7}$$

where $\gamma_i, i \in \{1,2\}$ denotes two independent closed paths (loops) on the torus which cannot be homotopically deformed into each other and μ_i are the Maslov indices of the paths corresponding to the number of turning points. We choose the loop γ_1 lying in the plane $t = 0$ whereas γ_2 is a path connecting a point (p, q) at time t with the same point at time $t + T$. Since there is no turning point in time, it is always possible to choose γ_2 such that $\mu_2 = 0$. After solving equation (5) for p_t on the quasi-energy shell

$$\varepsilon = \widetilde{H}(q, p, t, p_t) = \text{constant} \tag{8}$$

the quantization conditions adopt the form:

$$\begin{aligned} I_1 &= \frac{1}{2\pi} \oint_{\gamma_1} \omega^1 = \hbar(n_1 + \tfrac{1}{4}\mu_1) \qquad n_1 \in \mathbb{Z} \\ I_2 &= \frac{1}{2\pi} \oint_{\gamma_2} \omega^1 + T\varepsilon = \hbar n_2 \qquad n_2 \in \mathbb{Z} \end{aligned} \tag{9}$$

with the Poincaré–Cartan form

$$\omega^1 = p\,\mathrm{d}q - H\,\mathrm{d}t. \tag{10}$$

Since the variable p_t does not enter into the equations of motion, a shift of p_t by a constant shifts the quasi-energy but does not affect the structure of the quasi-energy shell and therefore not the value of the integrals of the Poincaré–Cartan form. This is a remarkable difference to general two-dimensional systems. An immediate consequence is that the second quantization condition (9) can be fulfilled for any quantum number n_2 yielding a quasi-energy which is only defined modulo $\hbar\omega$

$$\varepsilon_{n_1 n_2} = -\frac{1}{T} \oint_{\gamma_2} \omega^1 + \hbar\omega n_2 \tag{11}$$

in complete agreement with quantum mechanics. Futhermore it is of interest to observe that—although the chaotic states cannot be quantized by vortex tube techniques—the total number of these chaotic states can be determined. The vortex tube belonging to an outer regular state, say $n = 107$, does not only provide a semiclassical quantization of this particular state, but the phase integral also measures the total number of states (regular or chaotic) inside the vortex tube.

2.1. Numerical method using Poincaré's surface of section

A practical method of semiclassical quantization uses Poincaré's surface of section (see e.g. [14]). In a two-dimensional autonomous system one specifies two surfaces of section, e.g. planes defined by setting one coordinate equal to zero. While propagating in time a quasi-periodic trajectory generates in each surface of section an increasing number of points which ultimately fill a closed curve densely. These invariant curves are the paths along which the action integrals are evaluated. Such a computation has to be iterated for different initial coordinates and energies until the two quantization conditions are fulfilled simultaneously. As already pointed out, one-dimensional time-periodic systems require only a single quantization condition and a subsequent periodicity condition for determining the quasi-energy, which is a simplification compared to the case of a general two-dimensional systems. A natural choice for the surface of section is a plane $t = t_0$, i.e. the trajectory coordinates (p, q) at times $t = t_0 + nT$, $n \in N_0$. A calculation of a second Poincaré section is not necessary for a quantization of the vortex tube although it could be used in the subsequent computation of the second integral (11) and hence for determining the quasi-energy. If the motion in the phase space region under consideration is a rotation, the specification of a second surface of section would cause no problems; each plane defined by $q = q_0 =$ constant can be used. In contrast, in the case of a librational motion, such a simple specification of a surface of section will, in general, fail because the invariant torus can exhibit complicated, periodic deformations and spatial movements, such that it will not intersect the plane $q = q_0$ at every time. Especially in this case we propose to determine the quasi-energy by evaluating the action integral along a true trajectory, i.e. a solution of the equations of motion, as described later.

For an integrable system the phase space can be parametrized by action-angle variables. The classical motion on a 2-torus, specified by the two actions I_1, I_2, is determined by its frequencies ω_1, ω_2 and in the privileged angular coordinates appears to be rectilinear in time

$$\varphi_i(t) = \varphi_i(0) + \omega_i t \qquad i = 1, 2. \tag{12}$$

The time periodicity of the system already ensures that the second of the angle variables is given by $\varphi_2 = \omega t$, i.e. the frequency ω_2 coincides with the driving frequency ω, and hence

$$\omega_1 = \omega\Omega. \tag{13}$$

If the frequencies ω_1, ω_2 are incommensurable, i.e. the winding number

$$\Omega = \omega_1/\omega_2 \tag{14}$$

is irrational, then a trajectory winds densely around the torus and for any continuous function $f(\varphi_1, \varphi_2)$ on the torus its *time average* along a trajectory is equal to its *space average* [15, 16]:

$$\langle f \rangle = \frac{1}{(2\pi)^2} \int_0^{2\pi} \int_0^{2\pi} f(\varphi)\, \mathrm{d}\varphi = \lim_{\tau \to \infty} \frac{1}{\tau} \int_0^{\tau} f(\varphi(0) + \omega t)\, \mathrm{d}t. \tag{15}$$

For an irrational value of Ω it can be approximated arbitrarily close by rational numbers. If k/m is such an approximation, a trajectory started on the torus will almost close after m periods in time while winding nearly k times around the torus in the other direction. The trajectory is homotopic to a path consisting of m times the path γ_2 plus k times the path γ_1 (see figure 1). The action along the trajectory is hence approximatively given by

$$I(mT) = \frac{1}{2\pi}\int_0^{mT} (p\dot{q} - H(p,q,t))\,\mathrm{d}t + \frac{mT}{2\pi}\varepsilon \approx (kI_1 + mI_2). \quad (16)$$

This relation is exact in the limit $k, m \to \infty$ with $k/m \to \Omega$ and we obtain the precise result

$$\varepsilon = \omega_2 I_2 + \omega_1 I_1 - \lim_{m\to\infty} \frac{1}{mT}\int_0^{mT} L(q,\dot{q},t)\,\mathrm{d}t. \quad (17)$$

This equation expresses a time-averaged version of the Legendre transformation between the quasi-energy ε and the Lagrangian L. Inserting the expressions for the quantized actions (9) yields

$$\begin{aligned} \varepsilon_{n_1 n_2} &= \hbar\omega n_2 + \hbar\omega_1(n_1 + \tfrac{1}{4}\mu_1) - \langle L\rangle \\ &= \hbar\omega(n_2 + \Omega(n_1 + \tfrac{1}{4}\mu_1)) - \langle L\rangle. \end{aligned} \quad (18)$$

Since ε is defined only up to multiples of $\hbar\omega$, it is convenient to introduce an angle

$$\theta = \frac{T}{\hbar}\varepsilon = \frac{2\pi}{\hbar\omega}\varepsilon. \quad (19)$$

Equation (18) suggests performing the quantization in two steps:

(i) Compute a Poincaré section for different initial coordinates (p,q) until the quantization condition for I_1 is met.

(ii) Start a trajectory on this fixed torus, integrate the Lagrangian and determine the winding number Ω. Inserting these values into equation (18) yields the quasi-energy.

Two aspects of this procedure need further considerations. First there is the practical problem of determining the winding number Ω which will be discussed in section 3. Second, there is the notorious problem in torus quantization of non-integrable systems due to resonances. We will devote the following section to this problem.

2.2. *Quantization near resonances*

A resonance corresponds to a commensurable frequencies ω_1, ω_2 yielding a rational winding number

$$\Omega = \frac{\omega_1}{\omega_2} = \frac{k}{m} \qquad k, m \in \mathbb{N}. \quad (20)$$

In such a resonant case it is not possible to construct an invariant torus just by integrating a single trajectory sufficiently long in time. If the system under consideration is integrable, an invariant torus does exist but the Poincaré section

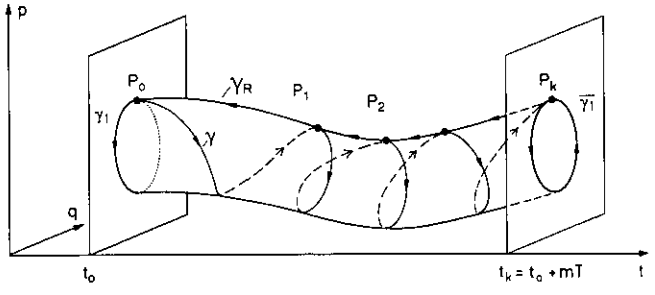

Figure 1. Periodic vortex tube in extended phase space. The trajectories starting on the invariant curve γ_1 sweep out the surface of a vortex tube and end at time $t_k = t_0 + mT$ on an invariant curve $\bar{\gamma}_1$ congruent to γ_1. Also drawn is a path of a single trajectory γ starting at P_0 winding k times around the vortex tube and ending at P_k, and a 'straight' retour path γ_R that connects the initial point with the final point without any winding. Evidently γ and γ_R intersect at exactly $k+1$ points $P_0, \ldots, P_k$ and thus form k oriented complete cycles c_i which can each be continuously deformed on the surface into γ_1. Hence the integral of the Poincaré–Cartan form along the sum of the two oriented paths $\gamma \oplus \gamma_R$ is the same as for the sum of the cycles c_i or k times the cycle γ_0.

of any trajectory consists only of m points, because all trajectories are periodic. In practice, this does not cause serious difficulties, since one can always find a nearby invariant torus with an irrational frequency ratio satisfying the quantization condition arbitrarily well. However, for a perturbed system, the KAM theorem tells us that the tori in the neighbourhood of a k/m resonance are usually destroyed and instead we find an island chain embedded in a stochastic layer. The centre of the islands are the intersections of an elliptic orbit of period m with the surface of section and in between one finds m hyperbolic fixed points, whose homoclinic intersections generate the chaotic motion around the islands. The area of this stochastic band depends on the strength of the perturbation and the denominator m of the frequency ratio (see, e.g., [17, 18]).

When trying to perform torus quantization for such a system one is faced with the problem that there is a countable number of such bands, corresponding to intervals in the action I_1, where no closed invariant curve exists. For weak perturbations when the resonance bands are narrow and do not overlap, it is possible to find invariant curves enclosing them and thus providing bounds for the action I_1. In such a case we still expect the torus quantization to yield reasonable results, if we use nearby tori and apply an interpolation technique which can be rigorously derived for the integrable case. Suppose we perform the calculation of the quasi-energy according to equation (18) not on the quantized torus but on a nearby torus with an action I_1 differing by ΔI_1 from the quantized one. Keeping now the quantized action I_2 fixed, ε can be regarded as a function of I_1 only. An interpolation formula can be derived by expanding ε in a Taylor series. The first derivative is given by the Hamiltonian equations in action-angle variables

$$\omega_i = \frac{\partial \widetilde{H}}{\partial I_i} \qquad i = 1,2 \tag{21}$$

leading to

$$\varepsilon(I_1 + \Delta I_1) = \varepsilon(I_1) + \sum_{j=1}^{\infty} \frac{\omega_1^{(j-1)}(I_1)}{j!} \Delta I_1{}^j. \tag{22}$$

The first derivative of ε with respect to I_1 obtained from equation (18)

$$\frac{\partial \varepsilon}{\partial I_1} = \omega_1 + I_1 \frac{\partial \omega_1}{\partial I_1} - \frac{\partial \langle L \rangle}{\partial I_1} \tag{23}$$

yields a relation between the derivatives of the frequency and the averaged Lagrangian when compared with the Hamiltonian equations (21)

$$\frac{\partial \omega_1}{\partial I_1} = \frac{1}{I_1} \frac{\partial \langle L \rangle}{\partial I_1} \tag{24}$$

which is given here for completeness. Considering now the quantized torus $I_1 + \Delta I_1 = \hbar(n_1 + \frac{1}{4}\mu_1)$, equation (22) gives in first order

$$\varepsilon_{n_1 n_2} = \varepsilon(I_1) + \omega_1 \Delta I_1 \tag{25}$$

which is nothing else other than a local harmonic oscillator approximation (see also [6]). Adding this correction term to equation (17), it takes the same form as equation (18) valid on the exact torus. This implies that the interpolation formula

$$\tilde{\varepsilon}_{n_1 n_2}(I_1) = \hbar \omega n_2 + \hbar \omega_1(I_1)(n_1 + \tfrac{1}{4}\mu_1) - \langle L(I_1) \rangle, \tag{26}$$

which uses the quantized action rather than the actual action I_1, already includes the first-order correction. In higher order we obtain

$$\varepsilon_{n_1 n_2} = \tilde{\varepsilon}_{n_1 n_2}(I_1) - \tfrac{1}{2} \omega_1'(I_1)(\Delta I_1)^2 + \mathcal{O}(\Delta I_1)^3. \tag{27}$$

There are two remarkable advantages of our quasi-energy formula (26):

(i) Only the data of a single trajectory are utilized to determine a quantizised quasi-energy in contrast to other approximation methods (see e.g. [4])).

(ii) Formula (26) requires no phase space area computation. This implies that one can use as well a resonant trajectory for determining the quantized quasi-energy, since $\langle L \rangle$ and $\Omega_1 = \omega \Omega$ are also well defined for such trajectories.

3. Numerical procedure

In order to determine the tori carrying quantized actions

$$I_1 = \hbar(n + \tfrac{1}{2}) \tag{28}$$

in the quasi-integrable region of phase space we compute numerically the symplectic area $\int \mathrm{d}p \wedge \mathrm{d}q$ inside the closed invariant curves and/or the line integrals $\int p \, \mathrm{d}q$ along the invariant curves. Each invariant curve intersects the q-axis twice so that the tori can be uniquely labelled, e.g. by $q_>$, which is the larger one of the intersection coordinates. In this way the actions are functions of a well defined variable $I = I(q_>)$ and the search for invariant curves satisfying (28) can be automated by an algorithm

like *regula falsa* or Newton's method. Newton's method would usually converge within 1% of $\hbar$ after only a few iterations except for those tori near resonances large compared to $\hbar$, which have to be found by trial and error. Once the quantized tori have been found the Lagrangian function can be integrated along a periodic or quasi-periodic trajectory to yield the 'average Lagrangian' $\langle L \rangle$ of equation (15). As a direct consequence of Poincaré's recurrence theorem a trajectory on the torus will eventually come arbitrarily close to its starting point. This ensures that for any starting point on the torus and any $\delta > 0$ there is a time $t_{m(\delta)} = m(\delta)T$, $m \in \mathbb{N}$, for which the trajectory is periodic within an error smaller than δ after which the computation is stopped. More precisely, there is an optimum way for approximating an irrational winding number by rationals, namely the series of its continued fraction approximants [17] k_j/m_j, $j \in I\mathbb{N}$ which converges like

$$\left|\Omega - \frac{k_j}{m_j}\right| < \frac{1}{m_j m_{j-1}} \tag{29}$$

in contrast to the inequality

$$\left|\Omega - \frac{k}{m}\right| < \frac{1}{m} \tag{30}$$

for an arbitrary approximation k/m. This shows that for a desired accuracy $\Delta\Omega$ of Ω the number of iterations necessary, is only of the order $1/\sqrt{\Delta\Omega}$. Hence, the use of a recurrence condition saves computation time compared to a fixed iteration limit. We emphasize that the determination of the winding number needs special care due to the high accuracy required especially for large quantum numbers n_1. For example when $n_1 > 100$ the quasi-energy formula (18) indicates that Ω has to be determined with an error less than 10^{-5} in order to achieve an accuracy of $10^{-3}\hbar$ for the quasi-energies. The use of this recurrence condition reduces the number of time periods necessary to about 10^3.

In case of a rotational motion in phase space a determination of the winding number is easy. If one had simultaneously calculated two surfaces of section each containing one of the independent paths γ_1, γ_2, one would simply take the ratio of the number of points in each surface of section. As already mentioned in section 2.1, this method using two surfaces of section will usually not work in the case of librational motion. In general the vortex tubes formed by the quantized tori will weave in a complicated manner through extended phase space (p, q, t) along the time axis (see figure 1). Thus the vortex tube *as a whole* can perform complete windings around a fixed reference line (p_R, q_R, t) which should not be mistaken as a winding on the torus itself.

The examples of a linearly forced and a parametrically excited [19] harmonic oscillator do not show such complications, because in these cases all vortex tubes remain straightly fixed in the q-direction and only oscillate in the p-direction. Another example studied by Breuer and Holthaus [8], a driven particle in a box, was treated only approximately in the adiabatic or low-frequency limit, where the need and difficulties of evaluating phase space integrals along paths of the *actual* vortex tubes could be circumvented.

For the general case, the following methods for determining the winding number on the torus are suggested:

1. Suppose there is a reflection symmetry in the surface of section whose symmetry axes intersects every torus twice. These two intersection points can be identified with the angles $\varphi_1 = 0$ and $\varphi_1 = \pi$, respectively. Counting the number $m(k)$ of times the point of intersection changes its orientation with respect to the symmetry line (i.e. the number of jumps across this line) while being iterated k times, we obtain an rational approximation for Ω. After k iterations the angle φ_1 has increased by $\varphi_1 = k\Omega$. In the case $0 < \Omega < \frac{1}{2}$ this implies that φ_1 has passed through 0 or π

$$m = [2k\Omega] \qquad \text{or} \qquad m = [2k\Omega] + 1 \tag{31}$$

times, depending on the initial angle. Here [ ] denotes the largest integer smaller than the argument. We thus obtain for the winding number:

$$\frac{m}{2k} < \Omega < \frac{m-1}{2k} \tag{32}$$

which obviously converges for large m. The proposed method does not distinguish between winding numbers which differ by an integer since they produce the same Poincaré map, as does the frequency $1 - \Omega$. This implies that the winding number cannot be uniquely determined by utilizing only the points in the surface of section; it is therefore necessary to determine the winding at least for one trajectory along its full length by a method like the following:

2. Take a reference trajectory *inside* the torus, preferably a periodic orbit, and draw a straight line from the reference trajectory *outward* to the chosen trajectory on the torus at any instant of time. Under the phase flow the so constructed line will rotate (not necessarily monotonically) in the (p, q)-plane and the average number of rotations in the limit of infinite time yields the winding number Ω. Another—maybe even better—way is by choosing two *different* trajectories on the torus, through which a line is drawn. Then the average number of *complete* rotations is an invariant property which is experienced by all such lines connecting two different trajectories on the torus. This follows from the observation that three different points A, B, C retain their relative ordering on the torus for all times, i.e. the trajectories which wind around the vortex tube cannot 'overtake' each other because of the uniqueness theorem for the equations of motion.

4. Results for a non-integrable system

As a model system we consider a forced quartic oscillator

$$H(t) = \frac{p^2}{2m} + bq^4 - \lambda q \cos(\omega t) \tag{33}$$

which is a special case of the classical Duffing Hamiltonian and was shown to be chaotic (see e.g. [20]). The system typically exhibits both regular and chaotic motion in coexistence as predicted by the KAM theorem. The special phase space structure of this coexistence depends on the four parameters, which are certainly not independent (in fact, three of them can be removed by rescaling). Recently, the quantum mechanical quasi-energies and Floquet eigenstates were studied for this system [11]. The authors distinguished between localized and non-localized Floquet

states and were able to relate them to three different regimes in classical phase space. Here we will analyse the quantum-classical relation in more detail by performing the EKB quantization as described earlier. As already mentioned in [11] for the parameter choice $m = 1$, $b = 1/4$, $\omega = 1$ and $\lambda = 1/2$ the phase space exhibits a clear separation into three different regions. The Poincaré section in figure 2 shows a central stability island embedded in a chaotic sea without further obvious island structures. This sea is again separated very clearly from the outermost area, which looks completely regular, i.e. the stochastic layers around rational winding numbers are so narrow, that they cannot be distinguished from invariant tori. This phenomenon is quite typical for all parameter values ($b > 0$), and has also been observed in other time-dependent systems (see, e.g., [21]). The details of the inner stability region, however, depend on the stability properties of the inner fixed point and do thus vary with the parameters. For our special parameter choice the winding number of the tori around the fixed point varies from $\Omega = 1.3963$ near the fixed point to $\Omega = 1.3765$ close to the border to the chaotic sea. A continued fraction expansion shows that a golden mean torus with $\Omega = 2 - (\sqrt{5} - 1)/2$ is contained in this interval whereas its first rational approximants ($\Omega = 3/2, 4/3, 7/5, 11/8$) are outside of this interval. A closer inspection of the border shows that it is dominated by two quite broad period-eight island chains, corresponding to the $11/8$ approximant of the golden winding number. The stability island hence corresponds to the winding number interval between the third and fourth approximant of the golden mean. Since there are no rational numbers with smaller denominators approximating the golden mean better than the continued fraction, this explains, according to the KAM theorem, why the stochastic bands inside the stable island are so narrow. The broadest of them will correspond to the fifth approximant of the golden mean ($\Omega = 18/13$).

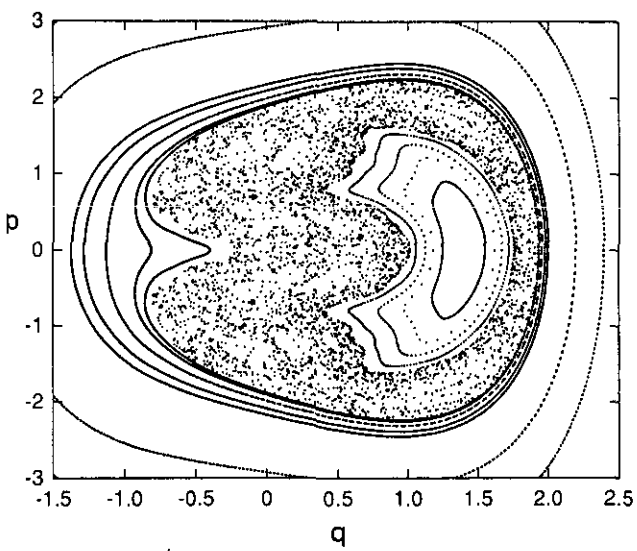

Figure 2. Poincaré surface of section for the Duffing oscillator (18) with parameters $m = 1$, $\omega = 1$, $b = 1/4$, $\lambda = 1/3$. Three regions in phase space can be clearly distinguished: an inner stability island, a chaotic sea and an outer quasi-integrable region.

4.1. Semiclassical and quantum quasi-energies

For comparison with quantum calculations the classical phase space will be measured in units of $h = 2\pi\hbar$ and the numerical values given later are for $\hbar = 0.015$ which was chosen in the quantum computations in [11]. Numerically, we determined the area of the stability island to be $23.65h$ if one excludes the period-eight island chain. Outside the island chain we still detected a single torus enclosing the inner stability island having an area of $27.28h$. Beyond this torus there are further island chains whose stochastic layers, however, do overlap thus preventing the existence of further closed tori. A trajectory started here is only separated by partial barriers (cantori) from the sea of global chaos. The area of the chaotic sea including the inner stability island is smaller than $104.7h$, which was computed from a numerically detected torus enclosing the chaotic sea. Concerning the quantum states, one could expect 23 'regular' states corresponding to the inner stability island, three or four states corresponding to the period-eight island chain and a number of 76–78 'chaotic' states. All further quantum-states belong to the outer almost regular regime and should hence be accessible to EKB quantization, thus allowing the attachment of semiclassical quantum numbers starting at about 104.

The results of the EBK quantization for the two regular regimes are presented in tables 1 and 2 in comparison with quantum mechanical results for the first 132 states. Notice that there exist no quantum numbers which can be attached to the quantum states. For convention the quasi-energy states have been ordered according to increasing values of the expectation value of $\langle H(t=0)\rangle$ and the listed number α of the states simply counts the states in this ordering, starting from $\alpha = 0$. In addition to the quasi-energy we have evaluated the classical average of the Hamiltonian at time $t = 0$, which can also be compared with the quantum result. In the tables only those states, attained semiclassically, are listed though the remaining 'chaotic' states, indicated by dots, were also determined quantum mechanically [11].

When surveying the tables the following remarkable observations can be made. First of all, the agreement between the semiclassical and quantum mechanical results is, for both the quasi-energy-phase θ and the averaged Hamiltonian, very good. One should keep in mind that θ is rescaled by $\hbar$ (see equation (19)), and by that its inaccuracies should not be compared with $\hbar$ but rather with 2π. For most of the values, the deviations are smaller than 10^{-3}, the only exceptions are some states in table 2 close to the border of the chaotic sea, where we find deviations which are larger by one digit.

Those states where the quantization condition could not be fulfilled within an error of $0.1\hbar$ in the action are marked by a '†'. Nevertheless, the interpolation formula (26) provides even in the latter case satisfactory results for the quasi-enegies. A closer inspection of the deviations in the values of θ shows that for the low states in table 1 most of the semiclassical values exceed their quantum mechanical counterparts whereas for the higher states in table 2 one can observe the contrary. These systematic deviations are due to the fact that equation (26) provides a linear approximation to the quasi-energy and equation (27) tells us that the sign of the second-order correction is opposite to the sign of the slope of the function $\Omega(I)$. Note that this function is monotonically decreasing in the inner stability region and increasing in the outermost region with a minimum at $I \approx 108$ (for a discussion of the role of the minimum in $\Omega(I)$ see [8, 21]).

Comparing α, the quantum mechanical denumeration of states, with the

Table 1. Lower quasi-energies $\theta = eT/\hbar$ arranged in increasing order of the average energy $\langle H(t=0)\rangle$ in comparison with results from the semiclassical EBK quantization. Also listed is the semiclassical quantum number n and the classical frequency ratio Ω.

Quantum mechanical			Semiclassical			
α	$\langle H(t=0)\rangle$	θ	θ	$\langle H(t=0)\rangle$	Ω	n
0	0.2702	3.1428	3.1425	0.2702	1.3963	0
1	0.2806	5.6304	5.6300	0.2806	1.3956	1
2	0.2911	1.8303	1.8282	0.2910	1.3948	2
3	0.3015	4.3090	4.3084	0.3015	1.3941	3
4	0.3120	0.5001	0.5006	0.3120	1.3934	4
5	0.3226	2.9699	2.9692	0.3226	1.3927	5
6	0.3332	5.4353	5.4343	0.3333	1.3920	6
7	0.3439	1.6130	1.6121	0.3439	1.3913	7
8	0.3546	4.0693	4.0689	0.3546	1.3906	8
9	0.3653	0.2378	0.2342	0.3653	1.3898	9
10	0.3759	2.6847	2.6837	0.3760	1.3891	10
11	0.3866	5.1266	5.1267	0.3867	1.3883	11
12	0.3972	1.2803	1.2796	0.3973	1.3874	12
13	0.4078	3.7118	3.7112	0.4079	1.3866	13
14	0.4184	6.1380	6.1385	0.4184	1.3857	14
15	0.4289	2.2753	2.2762	0.4289	1.3848	15
16	0.4397	4.6900	4.6901	0.4393	1.3839	16
17	0.4601	3.2187	3.2188	0.4599	1.3819	18
18	0.4702	5.6152	5.6143	0.4715	1.3808	19†
19	0.4769	0.8158	0.8152	0.4497	1.3829	17
20	0.4804	1.7220	1.7226	0.4803	1.3799	20
21	0.4905	4.1055	4.1054	0.4904	1.3788	21
22	0.5052	0.1991	0.1995	0.5006	1.3777	22
23	0.5107	2.5688	2.5702	0.5113	1.3765	23
24	0.5210	1.3518				
25	0.5459	2.9332				
26	0.5638	0.5966	0.5891	0.5366	1.3733	27†
27	0.5727	5.2811				
...	...	...				

semiclassical quantum number n one immediately notes that they coincide (apart from one exception) in the inner almost regular region up to number 23 and in the outer region from number 109 onwards. Close to the border to the chaotic sea, however, the quantum mechanical ordering fails, especially in the outer region (table 2). Here, the sequence of five regular states is interchanged and some chaotic states are mixed among them. The semiclassical quantization provides here a 'correct' ordering and hence a separation of 'regular' and 'irregular' states.

4.2. Density projections of tori and wavefunctions

For regular motion the classical trajectories are confined to a vortex tube, which appears in the Poincaré section as a smooth closed curve, a torus, which is invariant under the Poincaré map.

For the Duffing oscillator under study, tori in the (outer) quasi-integrable domain with quantum numbers $n > 116$ form convex invariant curves in the (p, q)-plane. The tori closer to the chaotic sea with $104 < n < 116$ develop a concave 'nose'. Characteristic examples are shown in figure 3 for the states $n = 0$, 105, 107 and 131. The classical phase space tori have a close resemblance in quantum mechanics. Figure

Table 2. Higher quasi-energies $\theta = \varepsilon T/\hbar$ arranged in increasing order of the average energy $\langle H(t=0)\rangle$ in comparison with results from the semiclassical EBK quantization. Also listed is the semiclassical quantum number n and the classical frequency ratio Ω.

Quantum mechanical			Semiclassical			
α	$\langle H(t=0)\rangle$	θ	θ	$\langle H(t=0)\rangle$	Ω	n
...	...	...				
93	1.0150	1.0963	1.1198	1.0169	1.1946	107
94	1.0193	6.1389	6.1507	1.0227	1.2027	106
...	...	...				
97	1.0298	4.8484	4.8577	1.0319	1.2099	105
...	...	...				
101	1.0414	3.5063	3.5162	1.0400	1.2154	104 †
102	1.0417	2.3091	2.3256	1.0359	1.1931	108
...	...	...				
109	1.1150	3.5698	3.5696	1.1102	1.2074	109
110	1.2048	4.9492	4.9463	1.2062	1.2305	110
111	1.2841	0.1780	0.1728	1.2852	1.2506	111
112	1.3502	1.8060	1.8014	1.3509	1.2675	112
113	1.4065	3.5319	3.5279	1.4070	1.2818	113
114	1.4560	5.3419	5.3386	1.4569	1.2945	114
115	1.5006	0.9429	0.9390	1.5013	1.3055	115
116	1.5417	2.8935	2.8917	1.5403	1.3151	116
117	1.5801	4.9049	4.9033	1.5806	1.3248	117
118	1.6164	0.6892	0.6887	1.6153	1.3331	118
119	1.6510	2.8089	2.8078	1.6513	1.3415	119
120	1.6842	4.9779	4.9774	1.6853	1.3493	120
121	1.7163	0.9104	0.9086	1.7172	1.3564	121
122	1.7474	3.1704	3.1688	1.7479	1.3633	122
123	1.7777	5.4728	5.4714	1.7782	1.3698	123
124	1.8073	1.5328	1.5316	1.8088	1.3764	124
125	1.8362	3.9153	3.9143	1.8365	1.3824	125
126	1.8647	5.2594	5.1655	1.8649	1.3883	126
127	1.8927	2.5098	2.5088	1.8927	1.3939	127
128	1.9204	5.0028	5.0027	1.9204	1.4000	128
129	1.9477	1.2473	1.2466	1.9481	1.4051	129
130	1.9746	3.8089	3.8083	1.9750	1.4104	130
131	2.0013	0.1203	0.1199	2.0019	1.4157	131

4 shows as an example the Husimi phase space density, i.e. a locally Gaussian (width $\hbar/2$) smoothed phase space distribution, for the quasi-energy state $\alpha = n = 107$. This quantum density clearly follows the classical phase space torus shown in figure 3. Most interestingly, one observes a pronounced quantum localization in phase space in the vicinity of the 'nose' of the classical invariant curve, where also the classical density accumulates (note the logarithmic scaling of the contours drawn in figure 4).

The classical density in position space, ρ_q, is computed by sampling the positions $q(t_n)$ of the trajectory following the quantizing vortex tube at times $t = t_n = nT$ in a histogram. The resulting distribution is the projection of the phase space torus in the stroboscopic Poincaré map onto position space (note that the density on such a torus is not uniform). At the critical points of this projection, the caustics, the projection is vertical giving rise to square root singularities in the classical densities. Note, that the classical momentum, $p_j(q)$, is generally a multivalued function, whose different branches, j, are connected at the critical points.

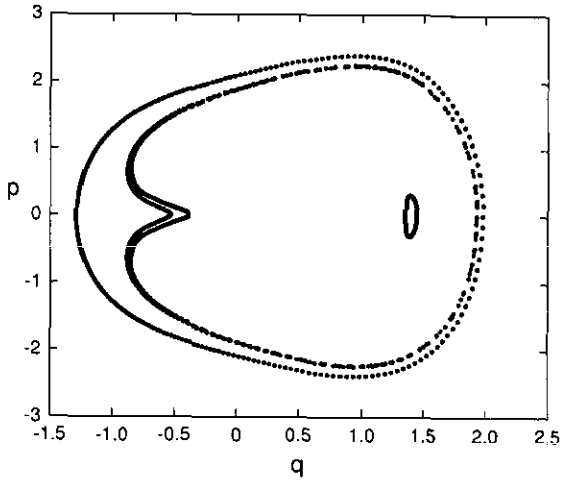

Figure 3. Four quantized tori with semiclassical quantum numbers $n = 0$, 105, 107 and 131 for which density profiles were calculated. The tori with $n = 0$ and $n = 131$ are convex and have only two caustics. The tori with $n = 105$ and 107 have both a concave 'nose' giving rise to a third caustic.

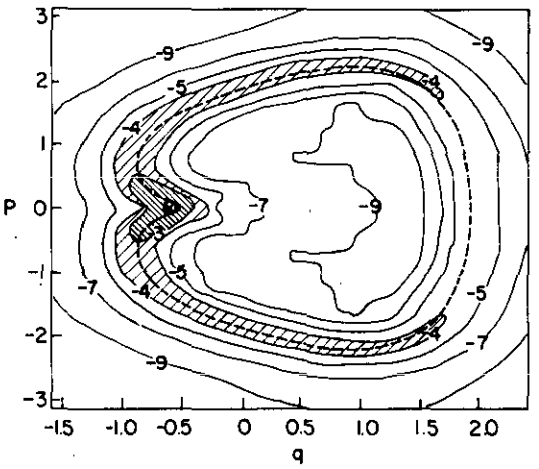

Figure 4. Quantum mechanical Husimi phase space density for quasi-energy state $n = 107$ ($\alpha = 93$), which is extremely localized in phase space. Contour lines of the densities on a logarithmic scale at values 10^{-3}, 10^{-4}, ... in arbitrary units are shown. The density at the maximum (marked by a cross) is 3.3×10^{-2}. The corresponding classical torus (compare figure 3) is shown as a broken curve.

The quantum mechanical density $\varrho_{qm} = |\psi|^2$ has an oscillatory structure due to the nodal lines of the wavefunction. Nevertheless, one can construct comparable 'coarse-grained' classical and quantum mechanical densities $\tilde{\varrho}_{cl}$ and $\tilde{\varrho}_{qm}$, by taking local averages. The spatial densities of the quantum quasi-energy states in the integrable region compare well with the classical densities on the associated tori when both densities are folded with a Gaussian of minimum uncertainty width $\sigma = \sqrt{\hbar/2}$. In the classical case this is equivalent to folding the invariant phase space density

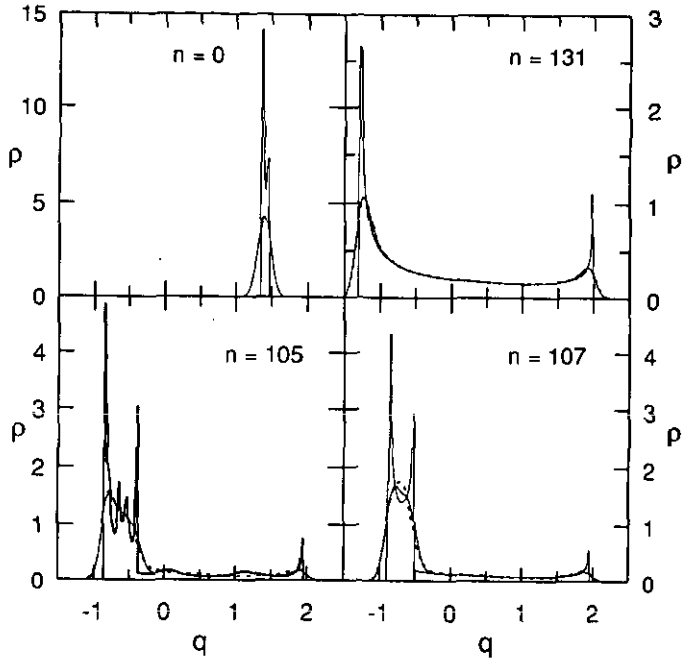

Figure 5. Classical and quantum mechanical density profiles. The classical density $\varrho_{\rm cl}(q)$ (peaky full curve), the Gaussian averaged classical density $\bar{\varrho}_{\rm cl}(q)$ (smooth dotted curve) and the Gaussian averaged density $\bar{\varrho}_{\rm qm}(q)$ (smooth full curve) of the quasi-energy states in position space are shown.

on the torus by a two-dimensional Gaussian and projecting the resulting averaged density onto configuration space. In the quantum mechanical case, this gives a Husimi distribution of the wavefunction projected down onto the q-axis. Typical classical and quantum mechanical density profiles are shown in figure 5. The basic skeleton of the classical densities is formed by the singularities resulting from vertical tangents to the phase space tori. For low ($n = 0$) and high ($n = 131$) regular states we have two singularities and for the lower states in the upper regular regime (e.g. $n = 105$ and 107) there are three such singularities (compare the phase space plots in figure 3). For tori, sufficiently far away from larger resonances, the classical and quantum mechanical coarse-grained densities agree extremely well, making it very difficult to distinguish the two profiles graphically (see figure 5). However, near resonances the classical density shows, in addition to the usual caustics, pronounced extra peaks. This is demonstrated in figure 5 for the state $n = 105$. These additional peaks result from a non-uniform accumulation of iterates of the Poincaré mapping near hyperbolic fixed points dividing the separatrix of a family of elliptic islands. In particular, when the invariant curve of the torus comes close to the stable or unstable manifold of the separatrix, the iterations will strongly accumulate towards hyperbolic fixed points as illustrated in figure 6. This effect can be amplified when the slope and curvature of the invariant curve changes drastically near the fixed point in such a way that the projected density onto the q-axis is increased. For the quantized torus with $n = 105$ a nearby chain of 17 small islands can be located. The q-coordinates of the separating

hyperbolic fixed points $H_1, \ldots, H_{17}$ coincide precisely with the positions of the extra peaks in the classical density in figure 5 for $n = 105$. Figure 7 finally shows an example of a non-smoothed wavefunction for the regular state number $\alpha = 93$ with semiclassical quantum number $n = 107$. In addition to the overall density profile already visible in the smoothed density shown in figure 5 one observes a regular pattern of almost equally spaced oscillations. Its spacing $\Delta q \approx 0.05$ agrees nicely with the semiclassical estimate $\Delta q \approx 2\pi\hbar/\bar{p}$ with $\bar{p}$ being the an average classical momentum during one oscillation (in the region $0 < q < 1.5$ we can use $\bar{p} \approx 2$, which gives $\Delta q \approx 0.047$).

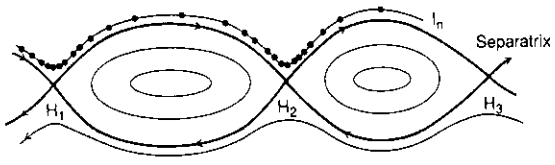

Figure 6. Quantized torus I_n near a resonance. The dots (•) represent iterates of the Poincaré mapping which accumulate near the hyperbolic fixed points H_1, H_2, ...

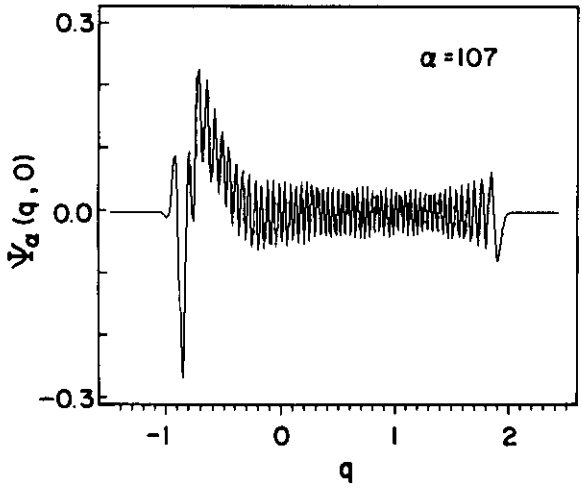

Figure 7. Quantum quasi-energy wavefunction $\psi_\alpha(q, t = 0)$ for state number $\alpha = 93$ with semiclassical quantum number $n = 107$.

5. Concluding remarks

It has been demonstrated in the present article that a considerable part of the quasi-enery spectrum of a forced anharmonic oscillator can be considered as regular, which implies that the states, which are found to be exponentially localized in state space, can be semiclassically quantized by EBK vortex tube quantization. The authors are

aware of the fact that the numerical procedure used in their computation may not be the most efficient one. Fourier transform techniques, for example, seem to be very promising, but such a development was not within the scope of the present study. More interesting, however, will be the derivation of a semiclassical description of the quasi-energy spectrum in the classically chaotic regime. This can be done in terms of Gutzwillers's periodic orbit theory [7]. Tabor [22] has developed such a formalism for semiclassically quantizing an area-preserving map. The extension of these methods to continuously driven systems are currently under investigation and will be addressed elsewhere.

Finally, we would like to point out that the results obtained for the somewhat specific example of a forced quartic oscillator can be extended to more general cases like the q^{2k}-oscillator [8] or to more realistic systems modelling field-induced transitions in molecular systems, as for instance a periodically forced rotor [23].

References

[1] Berry M V 1983 *Les Houches Summer School 1981 on Chaotic Behaviour of Deterministic Systems* ed G Iooss, H G Helleman and R Stora (Amsterdam: North-Holland) p 171
[2] Eckhardt B 1988 *Phys. Rep.* **163** 205
[3] Skodje R T, Borondo F and Reinhardt W P 1985 *J. Chem. Phys.* **82** 4611
[4] Ramaswamy R and Sinha S 1989 *Mol. Phys.* **67** 335
[5] Martens C C and Ezra G S 1985 *J. Chem. Phys.* **83** 2990
[6] DeLeon N and Heller E J 1983 *J. Chem. Phys.* **78** 4005
[7] Gutzwiller M C 1990 *Chaos in Classical and Quantum Mechanics* (New York: Springer)
[8] Breuer H P and Holthaus M 1991 *Ann. Phys., NY* **211** 249
[9] Ueda Y 1980 *New Approaches to Nonlinear Problems* ed H Bai-Lin, D H Feng and J-M Yuan (Philadelphia, PA: SIAM)
[10] Moon F C 1987 *Chaotic Vibrations* (New York: Wiley)
[11] Ben-Tal N, Moiseyev N and Korsch H J 1992 *Phys. Rev.* A **46** 1669
[12] Ben-Tal N, Moiseyev N, Fishman S, Bensch F and Korsch H J 1992 *Phys. Rev.* A in press
[13] Korsch H J and Berry M V 1981 *Physica* 3D 627
[14] Noid D W and Marcus R A 1975 *J. Chem. Phys.* **62** 2119
[15] Arnold V I 1978 *Mathematical Methods of Classical Mechanics* (New York: Springer)
[16] Percival I 1979 *J. Phys. A: Math. Gen.* **12** L57
[17] Berry M V 1978 *Topics in Nonlinear Dynamics (Am. Inst. Phys. Conf. Proc. 46)* ed S Jorna
[18] Lichtenberg A J and Lieberman M A 1983 *Regular and Stochastic Motion* (New York: Springer)
[19] Nuñez J A, Bensch F and Korsch H J 1992 *J. Phys. A: Math. Gen.* submitted
[20] Guckenheimer J and Holmes P 1983 *Nonlinear Oscillations, Dynamical Systems, and Bifurcations of Vector Fields* (New York: Springer)
[21] Breuer H P, Dietz K and Holthaus M 1990 *Physica* D **46** 317
[22] Tabor M 1983 *Physica* D **6** 195
[23] Moiseyev N, Korsch H J and Mirbach B 1992 *Phys. Rev.* A submitted